Microstructure of aragonite grown at an air–liquid interface

A. L. LITVIN*
Biotechnology Division, US Army Natick Research, Development and Engineering Center, Natick, Massachusetts 01760 and Geo-Centers, Inc., Natick, Massachusetts 01760, USA

D. L. KAPLAN
Biotechnology Center, Tufts University, Medford, Massachusetts 02155, USA

CHANGMO SUNG
Center for Advanced Materials, University of Massachusetts, Lowell, MA 01854, USA

Aragonite particles dispersed in a bioresorbable polymer matrix are considered to be a good candidate for bone prosthesis materials. It is important to characterize the microstructure of synthetic aragonite used for biomedical applications, since the microstructure may influence its integration, resorption and replacement by bone. We studied late stages of aragonite growth, at an air–liquid interface, from a solution not doped with additives. Comparison was made between the types of synthetic aragonite microstructure and that of aragonite which is found in nature (mollusc shells, gallstones, Earth's crust). The microstructure of natural aragonite is unique to certain classes of living organisms and the understanding of its structure/function relationships may help to select the types of synthetic aragonite for specific biomedical applications. Three types of synthetic aragonite were observed based on grain size and grain morphology.

1. Introduction

Aragonite, one of the $CaCO_3$ polymorphs, is found as a natural component in mollusc shells (exoskeleton) [1, 2], fish (gravity device) [1, 2], human brain stones [3], gallstones [4] and in the Earth's crust [5, 6]. Numerous studies have reported the synthesis of aragonite via the introduction of various inorganic and organic additives to calcium containing solutions and gels. For example, aragonite has been formed in the presence of NaCl and hexametaphosphate or pyrophosphate [7]. Metastable formation of aragonite in gels has been achieved at elevated pressure in a temperature range of 100 to 270 °C in the presence of Mg^{2+} [8]. Additives such as Mg^{2+}, Ni^{2+}, Co^{2+}, Fe^{2+}, Zn^{2+}, Cu^{2+} and Li^+ lead to aragonite growth at ambient conditions, and Sr^{2+}, Ba^{2+} and Pb^{2+} favour aragonite formation at high pH [9]. Aragonite also is a good material for biomedical applications since it is denser than calcite and could be integrated, resorbed and replaced by bone [10, 11]. Aragonite particles dispersed in a bioresorbable polymer matrix were used as a bone prosthesis material [12].

Recently, we reported a process of template-directed synthesis of aragonite from a calcium bicarbonate supersaturated solution not doped with additives [13]. Early stages of crystal growth were the focus of this work and the oriented nucleation of aragonite was achieved. The primary crystals were oriented with the [0 1 0] crystallographic axis perpendicular to the monolayer surface [13].

The present study is devoted to the later stages of aragonite growth, secondary nucleation, when the crystalline needles give rise to a splayed outgrowth into the supersaturated solution. While the microstructure and morphology of aragonite found in nature were studied extensively by transmission electron microscopy (TEM) [14, 15], the microstructure of synthetic aragonite were not fully characterized [14]. On the other hand, the microstructure is one of the most important features for bioceramics applications. The microstructure controls mechanical properties of ceramics, e.g. fracture toughness and elastic moduli [16]. It also influences the surface activity of bioceramics due to phase boundaries, missing grains or inclusions [17].

In this paper we study the types of synthetic aragonite microstructure and compare the morphology of natural and synthetic aragonite.

2. Experimental procedure

Synthetic aragonite was collected at the air–liquid interface on carbon coated copper TEM grids by gently dipping the grids through the monolayer. The

---

experimental setup for preparation of Langmuir monolayers has been described elsewhere [18–20]. The grids with samples were dried at ambient conditions for 1–2 days.

A Philips EM400T TEM equipped with LaB_6 was used to examine the microstructures and crystal structures of aragonite. The unit cell parameters and crystal symmetry were examined by electron microdiffraction and convergent beam electron diffraction (CBED) to determine local symmetry and three-dimensional crystallography of aragonite.

Compositional analysis of aragonite was carried out using the Noran Instrument 5500 low-Z energy dispersive X-ray spectrometry system (EDX). The following EDX parameters were maintained in the analysed areas: accelerating voltage of 120 keV, sample tilt of $12°$ and a Cl spot size setting of 4, giving an electron probe size of 20 nm. Dead time was in the range of 25% for the spectra collected.

3. Results and discussion

Several types of natural aragonite or its aggregates based on morphological descriptions were suggested in the literature. It has been reported that two different types of aragonite are found in gravelly sediments, i.e. acicular and bladed aragonite [21]. These types are similar in morphology to those found in tropical and subtropical environments [22]. Acicular crystals are equidimensional in cross-section and have pointed ends while bladed ones are transversely flattened and have blunt terminations. Another morphological classification has been reported for aragonite laminae aggregates found in hot water travertine crusts in Italy [6]. It was shown that the aragonite needle aggregates were in the form of crosses, fascicles (sheaf shaped bundles, or dumbbell shaped), rosettes and spherulites [6]. Another type of aragonite was found in nacre and had a blocky platelet morphology [15].

In our study, we observed at low magnification only acicular and spherulitic aragonite. The needle-like crystals (Fig. 1) develop from a common axis. We have characterized our synthetic aragonite by means of TEM observations of its microstructure at high magnification. We suggest that three types of aragonite could be distinguished based on its grain morphology. Grain size and morphology are of great importance for biomedical and bioengineering applications [17, 23].

Highly magnified images of the first type aragonite revealed grains in the form of very fine platelets which are directionally oriented, and are in the range of 2×40 nm in size (Fig. 2a). These features are typical of microlaminates associated with micropores in the grains and the overall texture represents a "ply-wood" structure [15, 24]. This "ply-wood" structure has been observed in nature for the cuticles of insects, crustaceans and spiders, and resembles that of a fibre-reinforced polymer matrix [15, 24]. The polymer "fibres" are oriented parallel to each other [15]. In our first type of synthetic aragonite we observed similar parallel "fibres". Presumably, this type of aragonite outgrowth was in contact with an organic monolayer. Elemental analysis of this and two other types of aragonite revealed only Ca, C and O without other typical elements such as Mg and Fe. Selected area electron diffraction (SAED) patterns were taken from the aragonite grains and revealed relatively fine grains (Fig. 2b).

The granular shape of the second type of aragonite outgrowth can be seen in the bright and centred dark field images (Fig. 3). Grains in this aragonite type were about 70 nm in diameter and were randomly oriented.
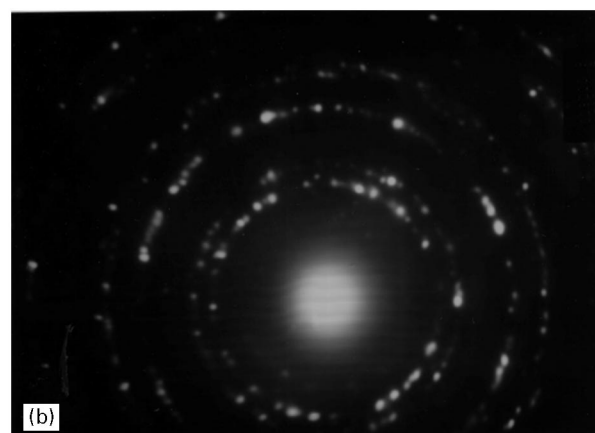

(a)   63 nm

38 μm

Figure 1 Aragonite imaged at low magnification on a TEM grid. The crystals develop from a common axis as needle-like.

(b)

Figure 2 (a) TEM image of the first type of aragonite. (b) Selected area electron diffraction pattern of the first type of aragonite (bottom).

A lower density of defects and micropores were observed in the grains. SAED patterns of [1 0 0] and [− 3 1 0] zone axes (Fig. 4) are indexed as aragonite (orthorhombic structure, SG = Pmcn (no. 62), a = 0.4959 nm, b = 0.7968 nm, c = 0.5741 nm). Computer simulated diffraction patterns were employed to confirm experimental aragonite patterns.

The third type of aragonite consisted of large grains (Fig. 5a). Individual grains are 0.5×1 mm in size. Each grain appears to be well developed crystallographically in three dimensions as seen from the centred dark field image (Fig. 5b). Faceted edges and fine twin structures were observed to overlap with thickness fringes (Fig. 6). Secondary nuclei of rectangular
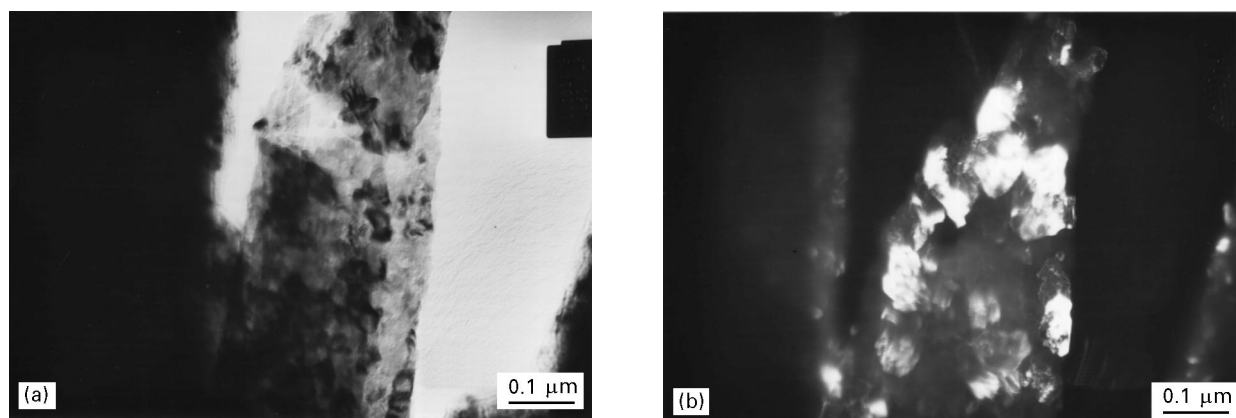

Figure 3 (a) TEM bright field image of the second type of aragonite. (b) TEM centred dark field image of the second type of aragonite.
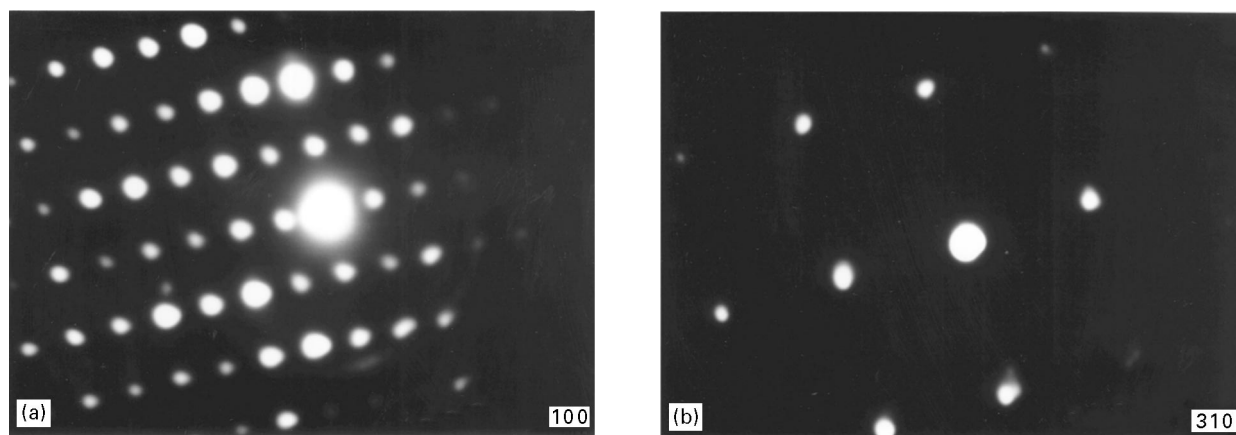

Figure 4 (a) Electron diffraction pattern of selected aragonite outgrowths. [1 0 0] zone of aragonite. Reflections: A = 0 2 2, B = 0 6 1, C = 0 4 − 1. Angles: (0 2 2) Λ (0 6 1) = 73.36°, (0 2 2) Λ (0 4 − 1) = 41.20°. (b) [3 1 0] zone of aragonite. Reflections: A = 1 3 2, B = 1 3 − 3, C = 2 6 − 1. Angles: (1 3 2) Λ (1 3 − 3) = 89.95°, (1 3 2) Λ (2 6 − 1) = 50.73°.
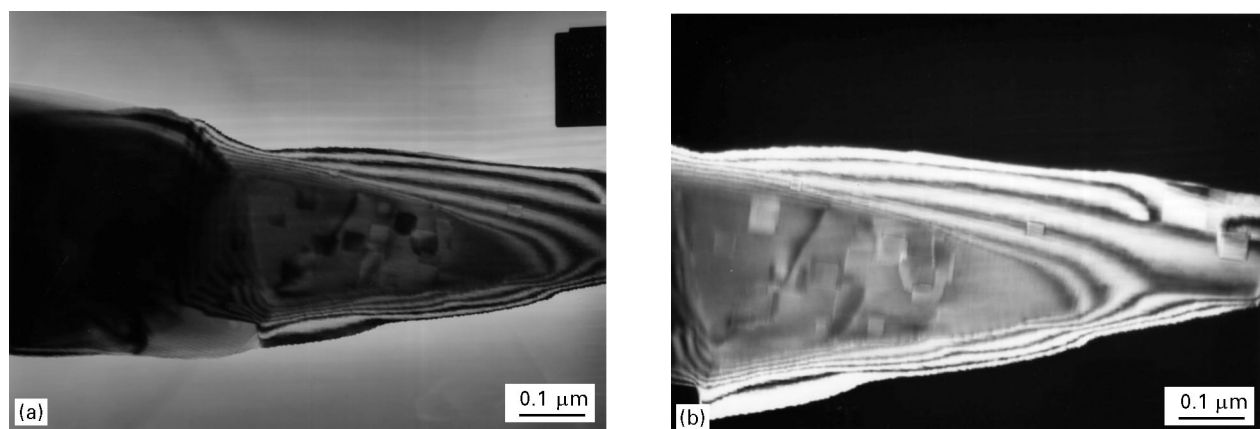

Figure 5 (a) TEM bright field image of the third type of aragonite. (b) TEM centred dark field image of the third type of aragonite.
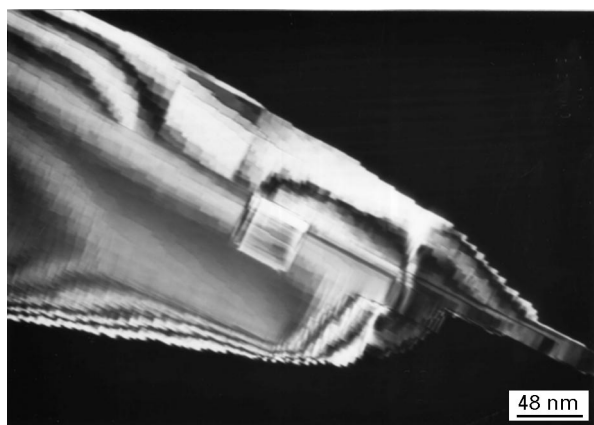
2235

Figure 6 Faceted edges and fine twin structure observed for the third type of aragonite.

or cubic geometry were found situated along the principal axis on several crystal grains. Similar secondary nuclei have been observed for intracellular crystals of aragonite in a species of the freshwater filamentous alga *Spirogyra* [25]. It was suggested [25] that the development of these nuclei into needle-like extensions with well-defined crystal ends and edges indicated a growth mechanism which results in discrete crystallographic faces being selectively enhanced.

4. Conclusion

Three types of synthetic aragonite were observed via TEM characterization of aragonite microstructure based on grain size and grain morphology. The first type of aragonite has very fine oriented "fibres" with grain size within 2×40 nm. It represents a "ply-wood" structure similar to one observed in nature for arthropod cuticles [15, 24]. The second type of aragonite has randomly oriented grains with grain size within 70 nm. The third type of aragonite also has randomly oriented grains with the biggest grain size of 0.5×1 mm. Secondary nuclei were observed to develop for this aragonite type similar to those seen in intracellular aragonite of *Spirogyra* [25].

The microstructure of natural aragonite is unique to certain classes of living organisms and the understanding of its structure/function relationships may help to select the types of synthetic aragonite for specific biomedical applications.

References

1. H. A. LOWENSTAM and S. WEINER, "On Biomineralization" (Oxford University Press, New York, 1989).
2. S. MANN (Ed.), "Biomimetic Materials Chemistry" (VCH, New York, 1996).
3. E. HONDA, M. AOKI, M. BUNNO and A. ITO, *Bull. Inst. Oceanogr. Monaco* **14** (1994) 115.
4. N. BASSI, G. FAVERO, T. MEGGIATO, P. SCALON, S. GHIRO, M. MOLIN, A. PILOTTO, S. VIGNERI, V. SAVARINO, G. S. MELA and F. DIMARIO, *Curr. Ther. Res.* **55** (1994) 1169.
5. A. PUTNIS, "Introduction to Mineral Sciences" (Cambridge University Press, Cambridge, 1993).
6. L. GUO and R. RIDING, *Sedimentology* **39** (1992) 1067.
7. T. F. BUEHRER and R. F. REITEMEIER, *J. Phys. Chem.* **44** (1940) 551.
8. W. A. FRANKE and N-A. MEHRAN, *Cryst. Res. Technol.* **27** (1992) 295.
9. M. OKUMURA and Y. KITANO, *Geochim. Cosmochim. Acta* **50** (1986) 49.
10. R. T. CHIROFF, R. A. WHITE, E. W. WHITE, J. N. WEBER and D. M. ROY, *J. Biomed. Mater. Res.* **11** (1977) 165.
11. A. L. LITVIN and D. L. KAPLAN, in Bioceramics 9, Otsu, Japan, November 1996, edited by T. Kokubo (Elsevier Science, Oxford, 1996) pp. 363–366.
12. P. CHRISTEL, French Patent No. 5, 433, 751 (1995).
13. A. L. LITVIN, S. VALIYAVEETTIL, D. L. KAPLAN and S. MANN, *Adv. Mater.* (1997) in print.
14. R. J. REEDER (Ed.), "Carbonates: Mineralogy and Chemistry" (Mineralogical Society of America, Washington, DC, 1990).
15. M. SARIKAYA, *Micros. Res. Tech.* **5** (1994) 360.
16. K. H. ZUM GAHR, "Microstructures and Wear of Materials", Tribology Series 10 (Elsevier, Amsterdam, 1987).
17. L. L. HENCH and J. WILSON (Eds), "An Introduction to Bioceramics" (World Scientific, Singapore, 1993).
18. A. L. LITVIN, L. A. SAMUELSON, D. H. CHARYCH, W. SPEVAK and D. L. KAPLAN, *J. Phys. Chem.* **99** (1995) 492.
19. A. L. LITVIN, L. A. SAMUELSON, D. H. CHARYCH, W. SPEVAK and D. L. KAPLAN, *J. Phys. Chem.* **99** (1995) 12065.
20. A. L. LITVIN, L. A. SAMUELSON, D. L. KAPLAN, C. SUNG, P. M. McCARTHY, D. H. CHARYCH and W. SPEVAK, in Proceedings on Smart Structures and Materials, San Diego, February 1995, edited by A. P. Jardine (SPIE, Bellingham, 1995) pp. 54–60.
21. A. E. ADAMS and K. SCHOFIELD, *J. Sediment Petrol.* **2** (1983) 417.
22. R. G. BATHURST, "Carbonate Sediments and Their Diagenesis" (Elsevier, Amsterdam, 1975).
23. E.g. the American Society for Testing and Materials, Philadelphia (ASTM) and Organization for Standardization (ISO) standards for alumina implants establish a limit of < 7 μm on mean grain size.
24. M.-M. GIRAUD-GUILLE, *Microsc. Res. Tech.* **5** (1994) 420.
25. H. MANN, S. MANN and W. S. FYFE, *J. Phycol.* **23** (1987) 506.